Supporting Information

Biophysical Influence of Airborne Carbon Nanomaterials on Natural Pulmonary Surfactant

*Russell P. Valle,[1] Tony Wu,[1] and Yi Y. Zuo[1,2]**

1. Department of Mechanical Engineering, University of Hawaii at Manoa, Honolulu, Hawaii 96822, USA

2. Department of Pediatrics, John A. Burns School of Medicine, University of Hawaii, Honolulu, Hawaii, 96826, USA

*** Corresponding Author**

Mailing Address: 2540 Dole St, Holmes Hall 302, Honolulu, HI, 96822, USA. Phone: 808-956-9650; fax: 808-956-2373; E-mail: yzuo@hawaii.edu.

List of Supporting Figures and Tables

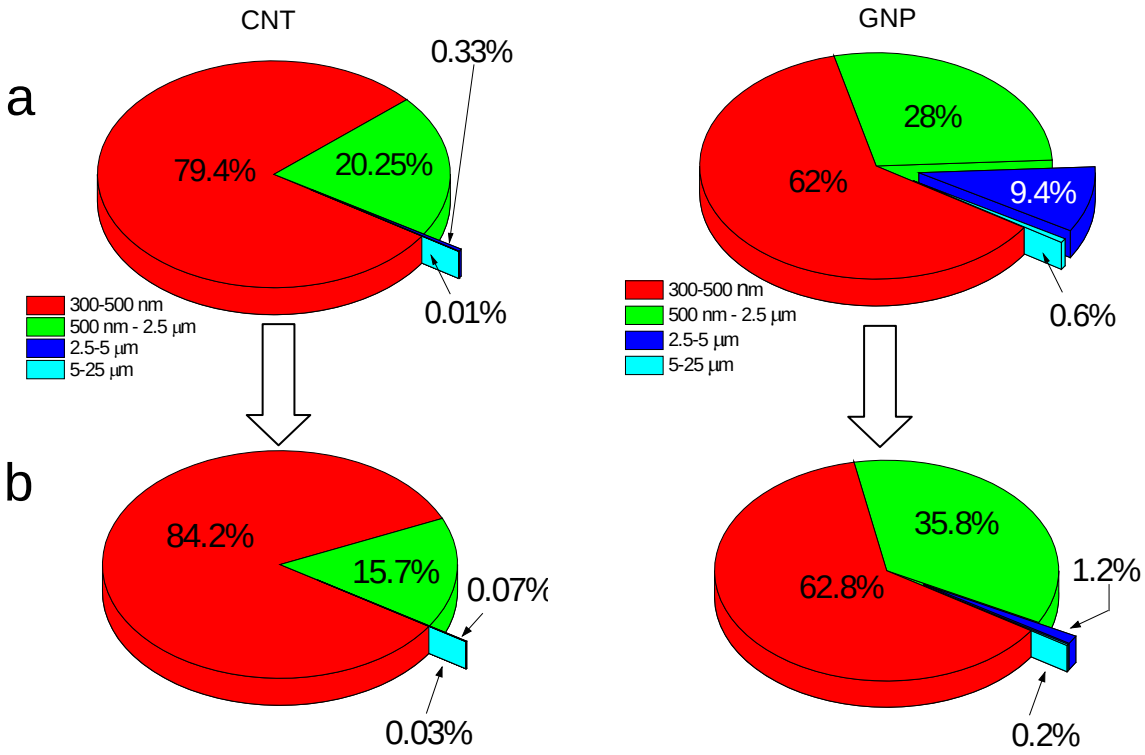

Figure S1. Size distributions of carbon nanomaterial (CNM) aerosols right after insufflation (a) and settling for 30 min after insufflation (b). For both carbon nanotubes (CNT) and graphene nanoplatelets (GNP), there are higher percentages of aerosols smaller than 2.5 µm after 30 min settling time than the initial insufflation.

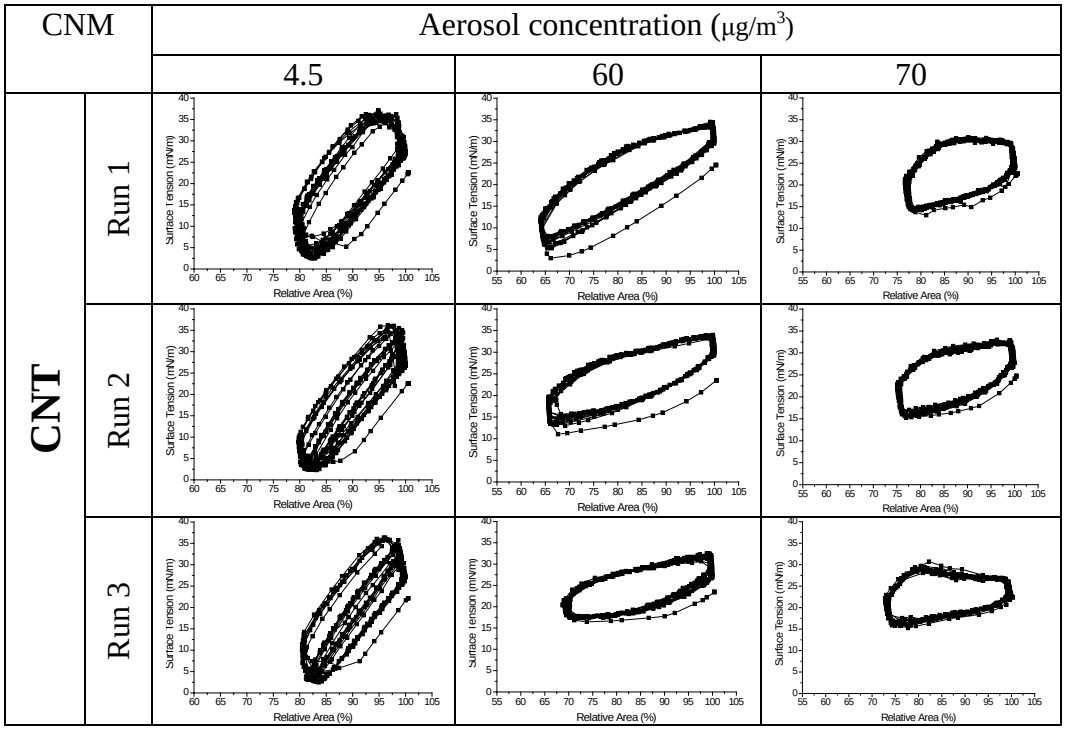

Figure S2. Reproducibility of dynamic cycling of Infasurf exposed to CNT aerosols. An Infasurf droplet was exposed to the CDS chamber containing 4.5, 60, and 70 μg/m^3 of airborne CNT. Quantitative analysis of surfactant inhibition, including γ_{min}, γ_{max}, κ_{comp}, and κ_{exp} shown in Fig. 4, was determined from these dynamic cycling data.

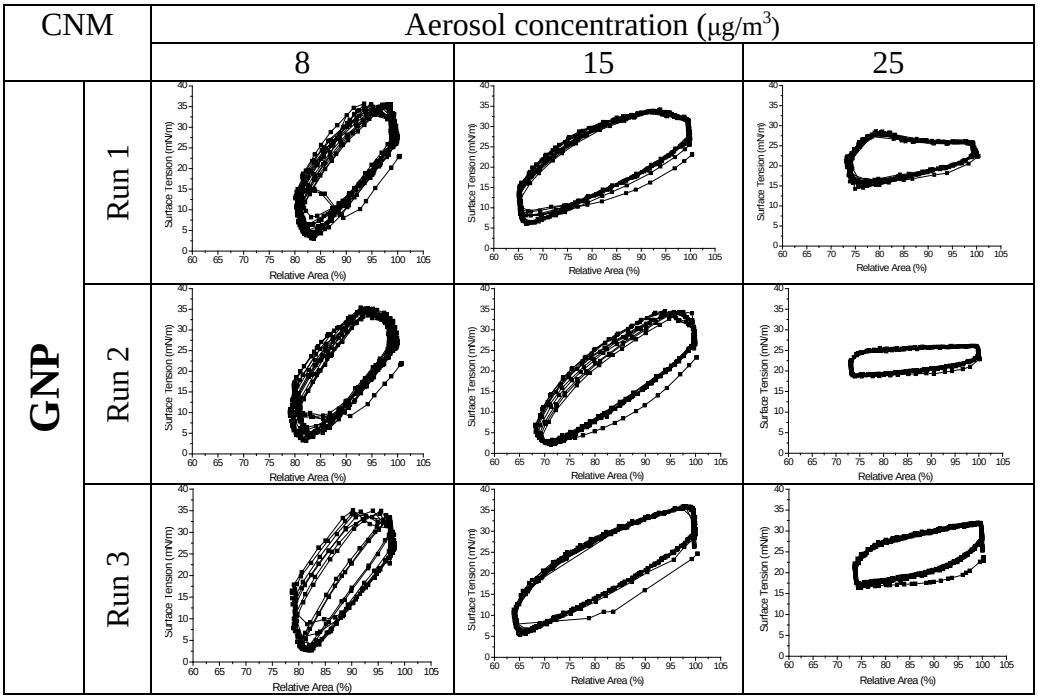

Figure S3. Reproducibility of dynamic cycling of Infasurf exposed to GNP aerosols. An Infasurf droplet was exposed to the CDS chamber containing 8, 15, and 25 μg/m^3 of airborne GNP. Quantitative analysis of surfactant inhibition, including γ_{min}, γ_{max}, κ_{comp}, and κ_{exp} shown in Fig. 4, was determined from these dynamic cycling data.

		50×50 µm	20×20 µm
Lateral		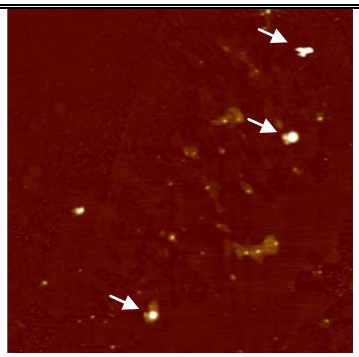	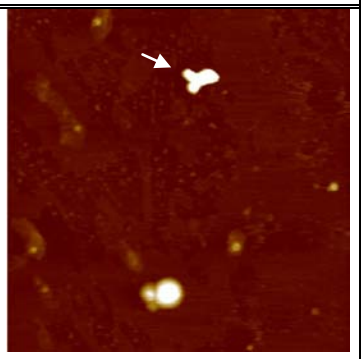
3-D		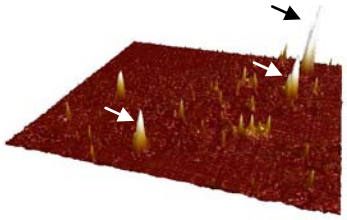	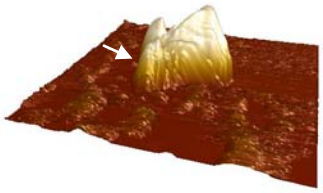
	100×100 µm	50×50 µm	10×10 µm
Lateral	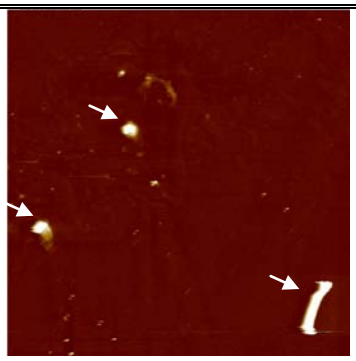	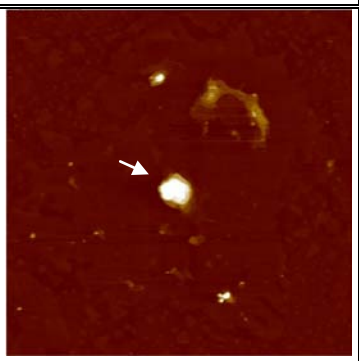	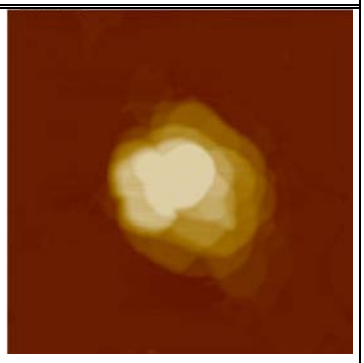
3-D	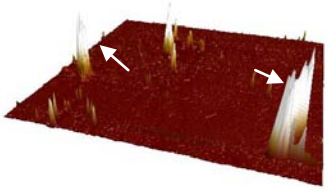	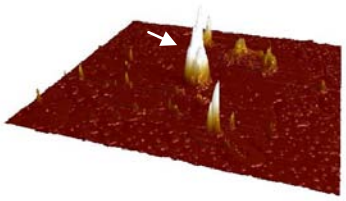	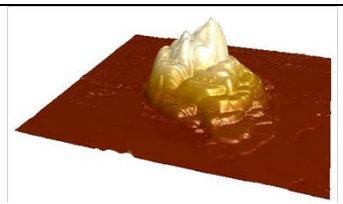

Figure S4. Additional AFM images of the Infasurf film exposed to CNT. Low and high resolution images show multiple particles per image noted by arrows. 3D images are given beneath each lateral structure image to give a contrast perspective of the height difference.

	100×100 µm	20×20 µm
Lateral	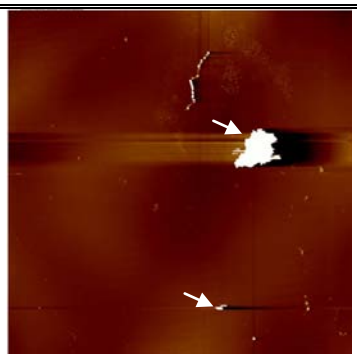	
3-D	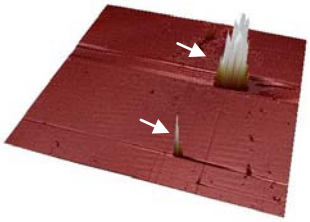	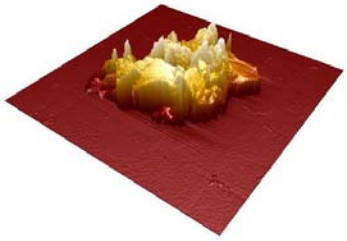
		10×10 µm
Lateral		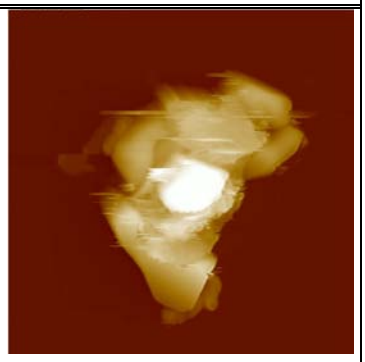
3-D		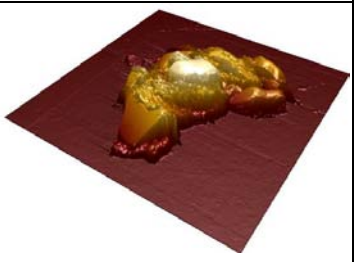

Figure S5. Additional AFM images of the Infasurf film exposed to GNP. Images show two positions where GNP particles were found. Both have similar morphology and heights of 1-1.5 µm. The low resolution image shows multiple particles noted by white arrows. 3D images are given beneath each lateral structure image to give a contrast perspective of the height difference.

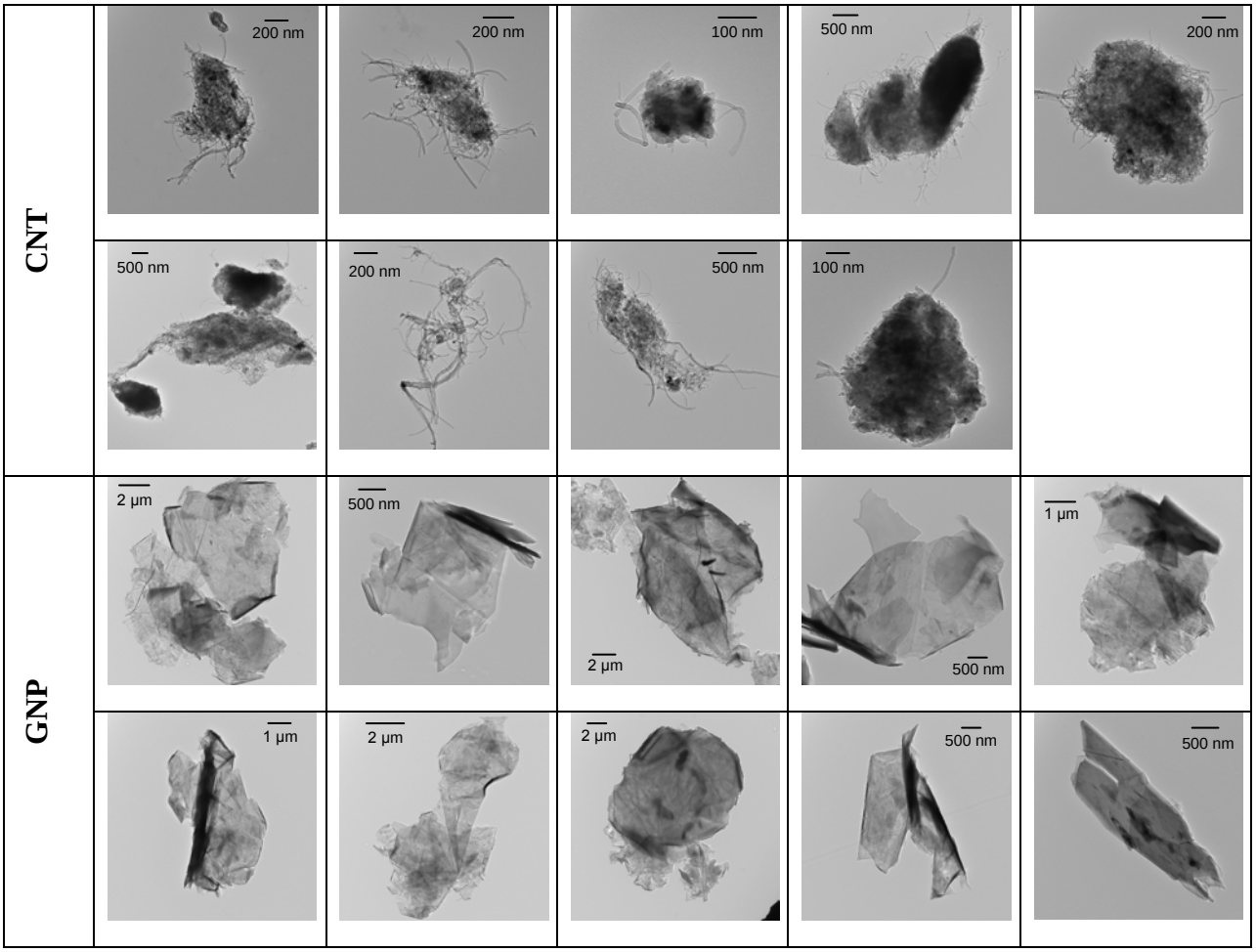

Figure S6. Additional TEM images for CNT and GNP aerosols, collected from the CDS chamber.

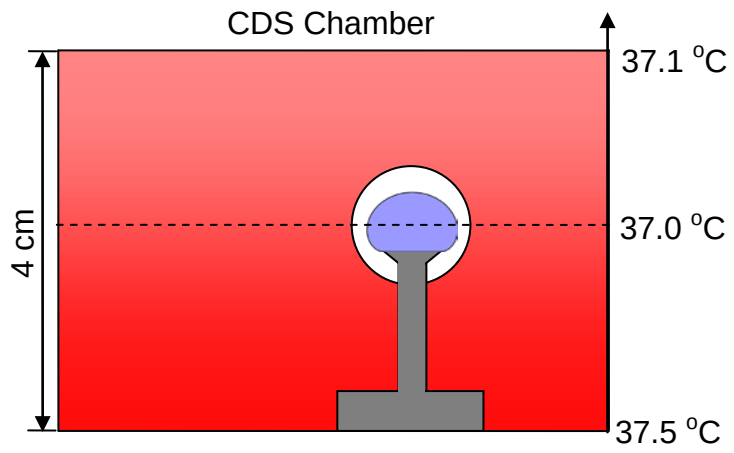

Figure S7. Temperature distribution within the CDS chamber.

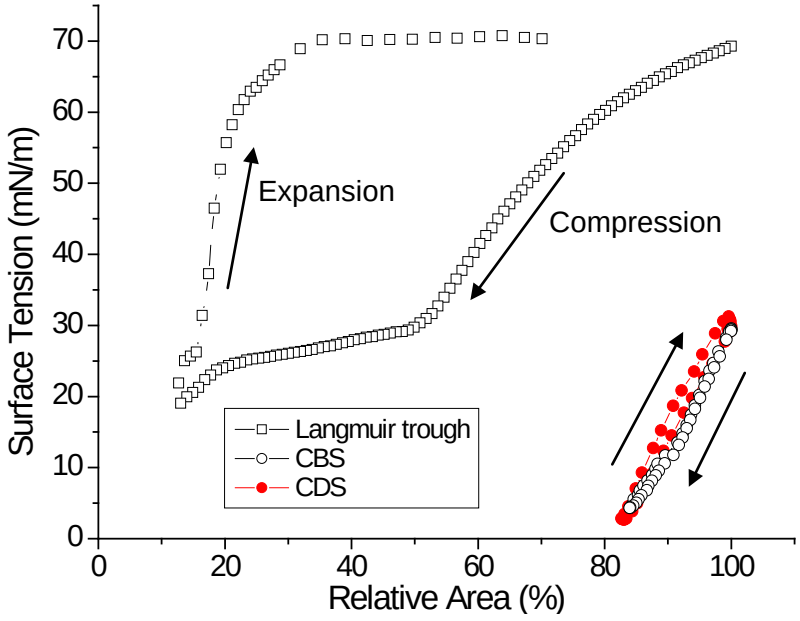

Figure S8. Comparison of the compression-expansion cycle of Infasurf recorded by the classical Langmuir trough (at room temperature), by the CBS and the CDS (at body temperature). It can be seen that the Langmuir trough fails to mimic the biophysical properties of natural PS. The CBS has been proven to be a benchmark for simulating biophysical properties of PS. We found an excellent agreement between the CBS and the CDS, proving that the CDS is able to reproduce biophysical properties of natural PS under physiologically relevant conditions. Moreover, the CDS used a much smaller surfactant reservoir than the CBS (~ 10 µL vs. > 1 mL). Meanwhile, design of the CDS makes it much easier than the CBS for studying airborne particles.

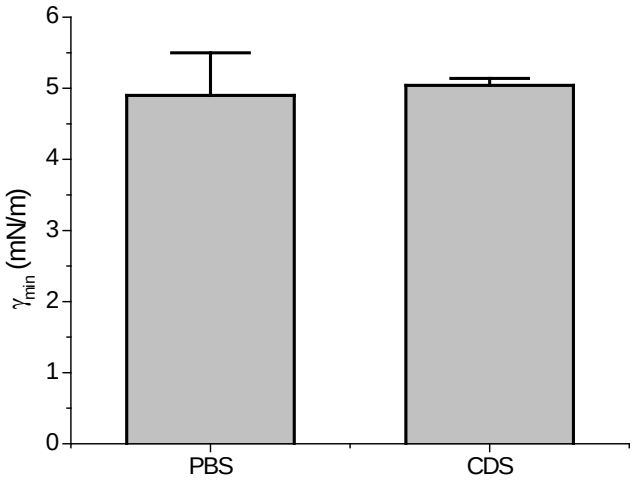

Figure S9. Comparison of the minimum surface tension (γ_{min}) of 1.5 mg/mL Curosurf determined under physiologically relevant conditions using the PBS (Schleh et al. *Respir. Res.* 2009, 10, 90) and the CDS. It is found that the γ_{min} determined by the two *in vitro* methods is very close, i.e., ~ 5 mN/m. This low surface tension is consistent with the high surface activity of natural PS.

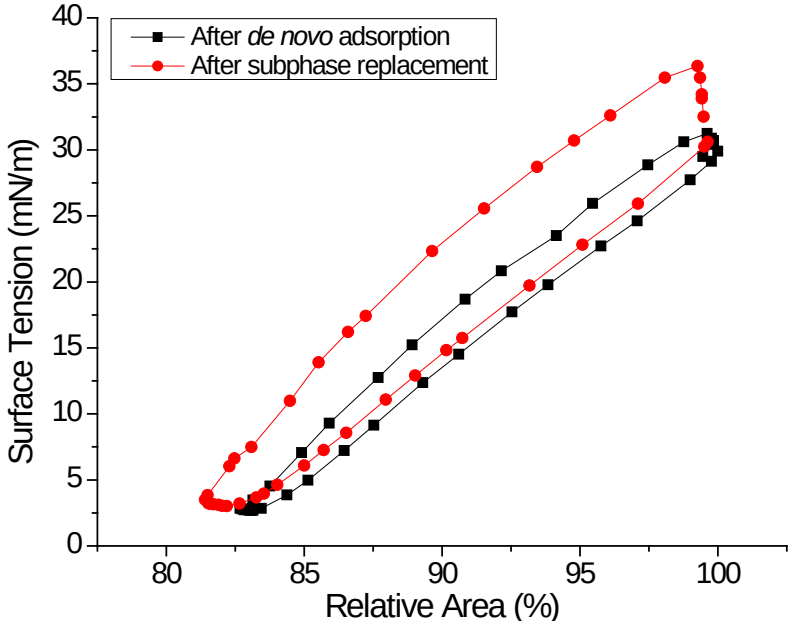

Figure S10. Subphase replaced Infasurf droplet biophysics showing no distinctive difference from *de novo* adsorbed film with vesicles in the subphase.

Table S1. Following the literature we used the following calculation to convert particle number concentration to mass concentration: $C=N\times(4/3)\pi r^3\times\rho\times V^{-1}$, where C is the mass concentration, N is the particle count, *r* is the average of size range, ρ is the particle density, and V is the total volume of the CDS chamber. The table outlines the mass contributions from three particle size ranges, measured with the laser diffration spectroscopy.

	Exposure Level	Trial	Particle Count				Mass Concentration Contribution ($\mu g/m^3$)			
			300nm - 500 nm	500 nm- 2.5 μm	2.5 - 5 μm	5 - 25 μm	300 nm -500 nm	500 nm - 2.5 μm	2.5 - 5 μm	5 - 25 μm
CNT	Low	1	191058	38171	1875	83	4.1	38	33	93
		2	224837	44914	5327	241	4.9	45	93	271
		3	208851	41720	3526	1412	4.5	42	62	1587
	Moderate	1	3358589	670912	7731	2481	73	680	135	638
		2	2210592	441588	7304	1570	48	447	128	1765
		3	2526103	504615	1215	543	55	511	21	139
	High	1	2285104	456473	1095	695	50	462	19	781
		2	3766302	752357	1545	187	82	762	27	48
		3	3634564	726041	4878	3277	79	735	85	3685
	Exposure Level	Trial	Particle Count				Mass Concentration Contribution ($\mu g/m^3$)			
			300nm - 500 nm	500 nm- 2.5 μm	2.5 - 5 μm	5 - 25 μm	300 nm -500 nm	500 nm - 2.5 μm	2.5 - 5 μm	5 - 25 μm
GNP	Low	1	441803	238940	19737	4124	9.2	277	346	4637
		2	425178	229949	16575	3313	8.9	267	291	3725
		3	287896	155703	14745	3180	6	200	259	3576
	Moderate	1	674253	364657	29723	4614	14	844	522	5188
		2	718141	388393	34175	5551	15	899	600	6246
		3	924058	499760	35188	6426	19	581	618	7226
	High	1	974891	527252	33256	9604	20	613	584	10800
		2	1499618	811040	1396	1551	31	943	24	1744
		3	968330	523703	38601	9938	20	609	678	11175

List of Supporting Video Clips

Video 1. Ambient air cycling. Infasurf droplet exposed to ambient air under compression and expansion cycling. Notice the droplet shape deformation to a flatter, non-spherical shape which correlates to lower surface tension.

Video 2. CNT exposure cycling. Infasurf droplet exposed to CNT under compression and expansion cycling. Notice the lack of shape deformation to a flatter, non-spherical shape which correlates with a lack of surface tension reduction, *i.e.* surfactant inhibition.

Video 3. GNP exposure cycling. Infasurf droplet exposed to GNP under compression and expansion cycling. Notice the lack of shape deformation to a flatter, non-spherical shape which correlates with a lack of surface tension reduction, *i.e.* surfactant inhibition.